A revised mesoscale wind farm model implemented in the Weather Research and Forecasting (WRF) code

HENNING HEIBERG-ANDERSEN* AND IDAR BARSTAD

Uni Research, Bergen, Norway.

ABSTRACT

Physical breaches in the wind farm models implemented in the current and previous versions of WRF have been identified. The affected variables are the the turbulent kinetic energy, the velocity tendencies and thus the power production of the wind farm. Therefore we have derived and implemented a new physically consistent wind farm model within the original framework developed at Uni Research. Development of the relevant variables through the Horn's Rev wind farm according to the the revised model and the one implemented in the current version of WRF are compared to measurements.

1. Introduction

Numerical mesoscale models with horizontal grid spacing of $\mathcal{O}$(1km) are central tools in producing wind climatologies and forecasts for offshore wind farms. Offshore wind farms have the potential to significantly affect atmospheric flows, see e.g. Smith (2009). In statically stable conditions, wind farm wakes may easily extend 50 km downstream and produce significant lateral disturbances. There is even a noticeable upstream impact from large offshore wind farms. Various wind farm representation exist for mesoscale flow models; from analytical collective wake estimates (Frandsen et al. 2006) to more complex formulations adding momentum drag and turbulence to the model equations as described by turbine type and geometry specifications (e.g. Jiménez et al. (2015)). For assessment of the mesoscale impacts of wind farms, naturally, the representation of the unresolved wind turbines is the core issue. Modelling of the subgrid turbine drag and the small-scale turbulence generated by the turbine blades in Planetary Boundary Layer (PBL) schemes is challenging.

Two wind farm models (Fitch et al. 2012; Jiménez et al. 2015) have previously been implemented in WRF. Both are based on the derivation of Blahak et al. (2010), which will be debated at several points as we formulate a revised model in the following sections. As in the preceding works, the wind farm model is implemented in conjunction with the modified Mellor-Yamada scheme of Nakanishi and Niino (2004) and the level of detail in the turbine modeling is weighted against expected visibility on the mesoscale. From this viewpoint, the rotor axes of the individual turbines are assumed to be constantly aligned with the mean horizontal wind direction at hub height, and drag from the towers supporting the turbines are ignored.

2. The revised model

In the following, Reynolds-averaged flow variables are called mean variables and denoted by uppercase letters, while their turbulent fluctuations are denoted by lowercase letters. Under the Boussinesq approximation, the equation for the horizontal components of the mean wind speed then reads, in Einstein notation,

$$\frac{\partial U_i}{\partial t} = \frac{\partial}{\partial x_j}\left(\frac{1}{\rho}\overline{\tau}_{ij} - U_i U_j\right) - g[1-\gamma(T-T_0)]\delta_{i3}, \quad (1)$$

where U_i is the i'th component of the mean wind speed, ρ is the air density at the reference temperature T_0, γ is the thermal expansion coefficient, g is the constant of gravity and $\overline{\tau}_{ij}$, where the bar denotes Reynolds-averaging, is the effective stress experienced by the mean flow. The latter is given by

$$\overline{\tau}_{ij} = -Pr\delta_{ij} + \rho\nu\left(\frac{\partial U_i}{\partial x_j} + \frac{\partial U_j}{\partial x_i}\right) - \rho\overline{u_i u_j}, \quad (2)$$

where Pr is the mean pressure and ν is the air viscosity. The last term of $\overline{\tau}_{ij}$, where u_i is the i'th component of the turbulent velocity fluctuation, is the so-called Reynolds stress, originating from Reynolds-averaging of the nonlinear terms in the momentum equation.

*Corresponding author address: Uni Research, Nygårdsgaten 112, 5008, Bergen.
E-mail: Henning.Heiberg-Andersen@uni.no

a. Intuitive first order update of velocity tendencies

In the physics module of WRF, the affected field variables are computed at the cell centers (Skamarock and Coauthors 2008). When constant air density is assumed throughout the cell, the cell center (x^c, y^c, z^c) coincides with the center of mass of the air contained in the cell, and the speed of the mass center, U_i^c equals the average speed in the cell:

$$\begin{aligned} U_i^c &= \frac{1}{\Delta x \Delta y \Delta z} \int_{x^c-\Delta x/2}^{x^c+\Delta x/2} \int_{y^c-\Delta y/2}^{y^c+\Delta y/2} \int_{z^c-\Delta z/2}^{z^c+\Delta z/2} \\ &\times \; U_i(x,y,z,t) \\ &= \frac{1}{\Omega} \int d\Omega U_i, \end{aligned} \tag{3}$$

where $\Omega = \Delta x \Delta y \Delta z$ is the volume of the cell. WRF derives the cell center values of the velocities from the Arakawa C-grid by linear interpolation, and it is easy to show by Taylor expansion of the integrand in (3) that the equation

$$U_i^c = U_i(x^c, y^c, z^c, t) \tag{4}$$

holds if U varies linearly and the air density is constant throughout the cell. From Newton's 1. law, the i'th component of the force on the air in the cell is given by

$$F_i = \rho \Omega \frac{\partial U_i^c}{\partial t}, \tag{5}$$

where, again, ρ is assumed constant. If a mesoscale cell contains the entire rotor of a turbine located at its horizontal center, one can already anticipate the first order update of the native WRF code. It reads

$$\frac{\partial U_i^c}{\partial t} \longrightarrow \frac{\partial U_i^c}{\partial t} - \frac{T_i}{\rho \Omega}, \tag{6}$$

where T_i is the i'th component of the thrust T on the rotor. Since the rotor axis is assumed to be constantly aligned with the mean horizontal wind direction, we have

$$T_i = \frac{U_i^c}{U_a^c} T, \tag{7}$$

where

$$U_a^c = \sqrt{(U_1^c)^2 + (U_2^c)^2} \tag{8}$$

is the mean axial speed of the center of mass of the air contained in the cell.

However, inclusion of wind turbines in a WRF simulation is not as straightforward as the look of the first order update (6) suggests. The influence of some particular features of the PBL schemes applied in WRF as well as the shear size of the mesoscale simulation cell will be dealt with in the following subsections.

b. Formal first order update of velocity tendencies

The PBL solvers implemented in WRF apply the dimensionless η coordinates (Laprise 1992), which are functions of the hydrostatic pressure, in the vertical direction. The corresponding z coordinates in the ordinary spatial coordinate system are therefore time dependent in WRF. Taking the time derivative of (3) by application of the Leibnitz theorem gives

$$\begin{aligned} \frac{\partial U_i^c}{\partial t} &= -U_i^c \frac{\partial \Omega}{\partial t} + \frac{1}{\Omega} \int_\Omega d\Omega \frac{\partial U_i}{\partial t} \\ &+ \frac{1}{\Omega} \int_{x^c-\Delta x/2}^{x^c+\Delta x/2} dx \int_{y^c-\Delta y/2}^{y^c+\Delta y/2} dy \\ &\times \left\{ U_i(x,y,z^c+\Delta z/2) \frac{\partial}{\partial t}(z^c+\Delta z/2) \right. \\ &- \left. U_i(x,y,z^c-\Delta z/2) \frac{\partial}{\partial t}(z^c-\Delta z/2) \right\} \end{aligned} \tag{9}$$

for an ordinary simulation cell containing no wind turbines. The assumed linearity of the mean wind over the simulation cell implies

$$U_i(x,y,z^c \pm \Delta z/2, t) = U_i(x,y,z^c,t) \pm \frac{\Delta z}{2} \frac{\partial}{\partial z} U_i(x,y,z,t)|_{z=z^c},$$

which inserted into (9) gives

$$\frac{\partial U_i^c}{\partial t} = \frac{1}{\Omega} \int_\Omega d\Omega \frac{\partial U_i}{\partial t} + \frac{\partial U_i^c}{\partial z^c} \frac{\partial z^c}{\partial t}. \tag{10}$$

Insertion of (1) and application of Gauss' divergence theorem to (10) gives for the horizontal components of the wind speed

$$\frac{\partial U_i^c}{\partial t} = \frac{1}{\Omega} \int_A dA_j \left(\frac{1}{\rho} \overline{\tau}_{ij} - U_i U_j \right) + \frac{\partial U_i^c}{\partial z^c} \frac{\partial z^c}{\partial t}, \tag{11}$$

where A is the surface bounding the cell volume Ω and dA_j is the j'th component of the outward pointing normal vector to the surface area element $d\mathbf{A}$.

Now we consider a cell containing a turbine rotor of radius R, represented by an actuator disk occupying the volume $\Omega_D = A_D \Delta S$, where $A_D = \pi R^2$ is the area swept by the turbine blades and ΔS is the thickness of the disk along the rotor axis. According to (3), the center of mass velocity of the air inside the cell is

$$U_i^c = \frac{1}{\Omega} \int_{\Omega - \Omega_D} d\Omega U_i - \frac{1}{\Omega} \int_{\Omega_D} d\Omega U_i. \tag{12}$$

Letting $\Delta S \longrightarrow 0$ makes the last term of (12) vanish. Taking the time derivative of the remainder and ignoring nonlinear vertical variation of the wind speed gives

$$\frac{\partial U_i^c}{\partial t} = \frac{1}{\Omega} \int_{\Omega - \Omega_D} d\Omega \frac{\partial U_i}{\partial t} + \frac{\partial U_i^c}{\partial z^c} \frac{\partial z^c}{\partial t}, \tag{13}$$

in accordance with (10). The presence of the turbine has of course disturbed the assumed linearity of the wind speed and introduced an error trough the last term of (13), which will grow with the rate of change in hydrostatic pressure. Beyond that, the importance of this error can hardly be assessed within the current modelling framework. The first term of (13), on the other hand, assumes nothing about the mean wind, and so is still valid. Since the actuator disk area is assumed vertical, only the horizontal components of the wind speed are affected. Application of (1) and the divergence theorem as for the empty simulation cell gives

$$\begin{aligned}\int_{\Omega-\Omega_D} d\Omega \frac{\partial U_i}{\partial t} &= \int_A dA_j \left(\frac{1}{\rho}\overline{\tau}_{ij} - U_i U_j\right) \\ &+ \int_{A_D^{(-)}} dA_j \left(\frac{1}{\rho}\overline{\tau}_{ij} - U_i U_j\right) \\ &+ \int_{A_D^{(+)}} dA_j \left(\frac{1}{\rho}\overline{\tau}_{ij} - U_i U_j\right)\end{aligned} \quad (14)$$

when the thickness of the actuator disk is vanishing. Here the $(\pm)$ superscripts to A_D denotes the two opposite sides of the disk, and the integrated stress over these areas amounts to the i'th component of the drag exerted on the wind by the turbine, which equals $-T_i$. The pressure drop across the actuator disk contributes the main part of T. Since the disk is assumed infinitesimally thin, the velocity fluxes $U_i U_j$ are identical on its opposing sides, and their contribution to (14) cancel. Collecting terms gives the anticipated first order update

$$\frac{\partial U_i^c}{\partial t} \longrightarrow \frac{\partial U_i^c}{\partial t} - \frac{T_i}{\rho\Omega}.$$

The nonlinearity error in the last term of (13) was however not evident from the considerations of the previous section.

c. Thrust and power calculations

For simplicity and efficiency, the thrust exerted on and power produced by individual turbines are calculated from thrust and power coefficients provided by the turbine manufacturer. This approach is approximate because the thrust and power coefficients are obtained under upstream conditions of uniform wind speed and vanishing turbulence. More accurate thrust and power predictions for individual turbines under the actual conditions inside the wind farm could be obtained by e.g performing Blade Element Momentum (BEM) analyses or interpolating from a library of thrust and power values obtained by CFD simulations of single turbines for various upstream wind speed, shear and turbulence intensity. However, we expect the gain in accuracy to be obtained by these or other elaborate methods to be small in comparison to the inherent discretization error of the mesoscale model itself.

Under measurement conditions, the thrust coefficient C_T is defined through the equation (see any book on wind energy)

$$T = \frac{\rho}{2} C_T U_\infty^2 A_D, \quad (15)$$

where U_∞ is the uniform upstream wind speed, on which C_T depends, and A_D is the rotor disk area as defined in the previous subsection. Likewise, the power P produced by the turbine is given by

$$P = \frac{\rho}{2} C_P U_\infty^3 A_D, \quad (16)$$

where C_P is the power coefficient. To derive U_∞ from U_a^c, we make use of the approximate relationship between C_T and the axial induction factor a, defined as

$$a \equiv \frac{U_\infty - U_D}{U_\infty}, \quad (17)$$

where U_D is the axial speed at the rotor, averaged over the rotor disk area.

In the classical momentum theory of turbines (see e.g Burton et al. (2011)), only the pressure term of (2) is present. Application of (1) to an expanding stream tube along the rotor axis which has the cross section of the actuator disk at the rotor position gives

$$T = \rho(U_\infty - U_W)U_W A_W \quad (18)$$

in the steady state. Here U_W is the assumed constant velocity across the wake area A_W. It is further assumed that the net pressures force on the outer boundary of the stream tube is zero, which is confirmed by application of (1) to a large control volume containing the stream tube. When pressure is the only stress source it further follows from (1) that in the steady state

$$\rho \frac{\partial}{\partial x_j}(EU_j) = \frac{\partial}{\partial x_j}(PrU_j), \quad (19)$$

where E is the mean kinetic energy density and loss to potential energy is ignored. Applied in conjunction with mass conservation respectively to the described stream tube and the control volume, (19) gives two alternative expressions for the power P produced by the turbine:

$$P = \frac{\rho}{2}(U_\infty + U_W)(U_\infty - U_W)U_W A_W \quad (20)$$

and

$$P = TU_D. \quad (21)$$

The ignored potential energy term would not have made any difference here as the vertical velocity averages to zero over the both the stream tube and the control volume. Insertion of (18) in (20) and comparison with (21) gives

$$U_D = \frac{U_\infty + U_W}{2}. \quad (22)$$

From the definition of the induction factor, (17), it then follows that

$$U_W = (1-2a)U_\infty. \tag{23}$$

The latter implies that the classical momentum theory breaks down for $a \geq 0.5$. However, for a larger than about 0.4 the shear layer defining the boundary of the stream tube becomes unstable (Burton et al. 2011), and the wake extracts energy from the surrounding wind by entrainment. Under this condition, mass conservation no longer requires that

$$U_W A_W = U_D A_D, \tag{24}$$

and the classical momentum theory result for the thrust coefficient,

$$C_T = 4a(1-a), \tag{25}$$

and the power coefficient,

$$C_P = 4a(1-a)^2, \tag{26}$$

no longer follows from (15-23). Modern wind turbines vary the rotational speed in order to keep a in the vicinity of $1/3$. At this value, the power coefficient of (26) reaches its maximum of 16/27, known as the Lanchester-Betz limit.

To account for the fact that the wind turbine has a finite number of blades, and thus exerts a lower drag on the wind near the blade tips than at the center of the rotor disk, Prandtl introduced the so-called tip loss factor F to modify the thrust coefficient for moderate values of a:

$$C_T = 4a(1-a)F. \tag{27}$$

A common value of Prandtl's tip loss factor is $F = 0.9$. For induction factors larger than $a = 0.5$, there is considerable scatter in the measured thrust coefficients (Lock et al. 1926), and various empirical formulas (Glauert 1926; Wilson 1994; Burton et al. 2011) have been proposed. As pointed out in Buhl (2005), none of these can be joined smoothly to the classical result when the tip loss factor is included. This problem is easily resolved (Buhl 2005) by the parametrization

$$C_T = b_0 + b_1 a + b_2 a^2 \tag{28}$$

for $a \geq a_0$, where $a_0 \leq 0.5$. For $a = 1$, C_T should be equal to 2 (Burton et al. 2011) and the thrust expressions of (27) and (28), as well as their first derivatives, should be identical at $a = a_0$. These three requirements determine b_0, b_1 and b_2 in (28) as functions of a_0 and F. For $a_0 = 0.4$ and $F = 0.9$ the resulting thrust curve lies tolerably near the center of the scattered data for high induction factors (Buhl 2005). The thrust curve is now an invertible function f of the induction factor, such that

$$a = f^{-1}(C_T). \tag{29}$$

For moderate induction factors, the near wake region is generally described well by the classical momentum theory (Burton et al. 2011). Assuming homogenous upstream wind velocity U_∞, a good approximation to the cell average of the axial wind speed U^c, is then given by

$$U_a^c = \frac{1}{2}U_\infty + \frac{1}{2}\frac{U_\infty(A_N - A'_W) + U_W A'_W}{A_N}, \tag{30}$$

where A'_W is the part of the wake area that is inside the cell, and

$$A_N = \begin{cases} \Delta y \Delta z U^c / |U_1^c| \text{ for } |U_1^c| \geq |U_2^c| \\ \\ \Delta x \Delta z U^c / |U_2^c| \text{ for } |U_1^c| < |U_2^c| \end{cases} \tag{31}$$

is the part of the plane containing the rotor disk that is inside the cell. For simplicity, we use a constant near wake area,

$$A_W = 2A_D, \tag{32}$$

from which we extract A'_W. It follows from (17), (23) and (24) that (32) corresponds to the optimum induction factor value of 1/3. Application of (17) and (22) to (30) gives

$$U_a^c = \left(1 - \frac{A'_W}{A_N}a\right)U_\infty. \tag{33}$$

The induction factor and thus the upstream wind speed can now be obtained from the axial wind speed at the cell center and a table of thrust coefficients by iterative use of (29) and (33). The algorithm is as as follows:

$a(0) =$ arbitrary value between 0 and 1
for $i = 1,\ n$
$U_\infty = U_a^c \left(1 - \frac{A'_W}{A_N}a(i-1)\right)^{-1}$
$C_T = C_T(U_\infty)$ (read off the thrust coefficients table)
$a(i) = f^{-1}(C_T)$
end
$a = (a(n-1) + a(n))/2$

where n is the chosen number of iterations. As a function of the induction factor, the measured thrust coefficient is generally not identical to the approximate universal relation of (28). As a consequence, the iteration loop above will not converge in general, but cycle between two constant values after a certain number of iterations. Hence the subsequent averaging over these two values. With the upstream velocity finally found by (33), the thrust and power are calculated by calculated by (15) and (16).

By contrast, both the previous wind farm models implemented in WRF (Fitch et al. (2012) and Jiménez et al. (2015)) follow the procedure of Blahak et al. (2010), where the horizontal cell center velocity is used directly in (15) and (16). From (33) it follows that the resulting error increases with increasing horizontal resolution.

d. Distribution of thrust over swept vertical levels

The horizontal mesoscale grid lengths are typically several rotor diameters, while significantly tighter spacing of the η levels is required to resolve the part of the boundary layer containing the turbines. Usually the rotor plane is thus distributed vertically over multiple simulation cells. As a reference volume we chose

$$\Omega = \sum_k \Omega_k, \tag{34}$$

where the sum runs over the vertical indices of cells that contain fractions of the rotor area, and the volume of the k'th cell is

$$\Omega_k = \Delta x \Delta y \Delta z_k, \tag{35}$$

where Δz_k is the cell height. An update of the horizontal velocity tendency terms for the cell of vertical index k which is consistent with (6) reads

$$\frac{\partial U^c_{k,i}}{\partial t} \longrightarrow \frac{\partial U^c_{k,i}}{\partial t} - \frac{T_{k,i}}{\rho \Omega_k}, \tag{36}$$

where $T_{k,i}$ is fraction of T_i contributed by the fraction of the rotor which is inside of the k'th cell in the column. The required forcing balance,

$$\sum_k \Omega_k \frac{\partial U^c_{k,i}}{\partial t} = \Omega \frac{\partial U^c_i}{\partial t}, \tag{37}$$

can be obtained with any vertical thrust distribution satisfying

$$\sum_k T_{k,i} = T_i \tag{38}$$

applied in (36). Without any blade analysis available, we are only able to account for the tip loss. Prandtl's tip loss factor can be expressed as

$$F = \sum_k f_k \tag{39}$$

where f_k is the integral of Prandtl's tip loss function over the area of the k'th cell in the column. The corresponding thrust contribution is

$$T_{k,i} = \frac{f_k}{F} T_i. \tag{40}$$

In both the previous wind farm models implemented in WRF, as well as in Blahak et al. (2010), it is attempted to account for wind shear by differentiating the thrust and power coefficients across the rotor according to the wind speeds at the centers of individual cells in the column. That approach is in conflict with (37). In addition, the thrust and power coefficients apply to the whole rotor only, and is not subject to differentiation according to vertical positions across the rotor.

e. Turbulent kinetic energy

For convenience of the subsequent discussion we quote the full equation for the mean energy density following from (1):

$$\begin{aligned} \frac{\partial E}{\partial t} &= \frac{\partial}{\partial x_j}\left(\overline{\tau_{ij}} U_i - E U_j\right) - \rho g [1 - \gamma (T - T_0)] U_3 \\ &- 2\nu R_{ij} R_{ij} + \rho \overline{u_i u_j} \frac{\partial U_i}{\partial x_j}, \end{aligned} \tag{41}$$

where

$$R_{ij} = \frac{1}{2}\left(\frac{\partial U_i}{\partial x_j} + \frac{\partial U_j}{\partial x_i}\right). \tag{42}$$

The terms on the right hand side are respectively transport, loss to potential energy, direct viscous dissipation of the mean flow, and loss to turbulent kinetic energy (TKE). The last term reappears with opposite sign in the TKE equation, where it is called the shear production term. Since the tips of the turbine blades moves with high velocity, the gradients of the mean wind velocity are large at the boundary of the rotor disk. Thus the shear production of TKE is large in this region. Due to the large size of the mesoscale simulation cells, the modest mean speed gradients produced by the native WRF code, even with first order turbine forcing, are not even remotely resembling the shear produced at the boundary of the rotor disk. Consequently, the simulated TKE production is far too small. The TKE inside the wind farm counteracts wake shadowing by mixing down fresh momentum from the air above. Insufficient TKE in the model will therefore result in a too steep decline in power along the farm in the mean wind direction.

According to (41), the rate of TKE production by a turbine inside a control volume V equals

$$\int_V dV \left(-\rho \overline{u_i u_j} \frac{\partial U_i}{\partial x_j}\right) = \int_A dA_j \left(\overline{\tau_{ij}} U_i - E U_j\right) \tag{43}$$

in the steady state when the viscous dissipation of the mean flow is ignored and the upstream wind is unform and horizontal such that the vertical velocity averages to zero over V. The viscous dissipation term vanishes except in the vicinity of the turbine where the flow is turbulent and its ratio to the shear production term can be estimated as $\mathcal{O}(\nu/\rho UL)$, where L is the turbulence length scale. Near the turbine L is of the same order as the rotor radius, so above cut-in wind speed the ratio of direct viscous dissipation to TKE production is of the order of 10^{-5}. The first part of the surface integral of (43) equals the work exerted on the mean flow by surface forces. Since ideal conditions of vanishing ambient turbulence and uniform ambient pressure is assumed, the net rate of work done on the outer boundary of the control volume is zero. Only the

rate of work done on the flow by the actuator disk representing the turbine remains, which means that

$$\int_A dA_j \overline{\tau_{ij}} U_i = -P. \tag{44}$$

Assuming the control volume is large enough that the stream lines are parallel to the upstream velocity U_∞ at the lateral boundaries, we get for the second part of the surface integral of (43)

$$\begin{aligned} \int_A dA_j E U_j &= \frac{\rho}{2} U_\infty^2 \int_A dA_j U_j \\ &+ \frac{\rho}{2} \int_{A_W} dA_1 (U_1^2 - U_\infty^2) U_1, \end{aligned} \tag{45}$$

where the first term on the right hand side is zero by mass conservation. If we assume the speed to be constant across the wake we obtain

$$\int_A dA_j E U_j \simeq -T U_D$$

as in the classical momentum theory. In this approximation the TKE production rate of the turbine equals $TU_D - P$, which, according to (21), is consistent with the fact that there is no TKE production in the classical momentum theory.

As is well known, the viscous dissipation rate ε of the TKE is, contrary to the direct dissipation of the mean energy, significant and of the same order of magnitude as the production of TKE by shear or buoyancy (Kundu and Cohen 2008). In the vicinity of a turbine we assume that shear production dominates, such that for each turbine in the farm

$$\alpha\rho \sum_k \int_{\Omega_k} d\Omega_k \varepsilon = T U_D - P, \tag{46}$$

where the sum runs over the column of cells inside the range of the rotor and α is a proportionality constant. At this point we encounter a dilemma. As mentioned in section 2a, the physics module of WRF use the cell center values of all fields. Since the shear production of TKE is concentrated at the boundaries of the rotor disk, application of (46) therefore misplace the dissipation for all cells in the column except the lowest and the highest. We see no perfect solution to this, but have chosen override the TKE production rate in these two cells by identical shares of the turbines shear production and leave the TKE of the remaining cells to the native WRF code. This implies no substantial double counting, since the TKE produced by the PBL scheme is comparatively insignificant. Hence, instead of (46), we apply

$$\alpha\rho \int_{\Omega_k} d\Omega_k \varepsilon = (T U_D - P)/2 \tag{47}$$

for highest and lowest cell in the column only. Then we can define the average dissipation rates for these cells as

$$\varepsilon_k^c = \frac{1}{\Omega_k} \int_{\Omega_k} d\Omega_k \varepsilon = \frac{T U_D - P}{2\alpha\rho\Omega_k}. \tag{48}$$

The final assumption is that these cell averages obey Prandtl-Kolmogorov formula for the turbulence length scale:

$$L = C_\varepsilon \frac{q^{3/2}}{\varepsilon}, \tag{49}$$

where $C_\varepsilon \simeq 0.168$ (Schlichting and Gersten 2000) and

$$q^2 = u_i^2 = \frac{2TKE}{\rho}, \tag{50}$$

which is known as "*qke*" in the WRF nomenclature. The cell average of q for the upper and lower cell is then obtained as

$$q_k^c = \left(\frac{T U_D - P}{2\rho C_\varepsilon \Omega_k} L \right)^{1/3}, \tag{51}$$

where we have absorbed the unknown proportionality constant α into the unknown turbulence length scale L, which remains the only adjustable parameter in this work. In the test simulations of section 3, L is set equal to the rotor radius. The expression of (51) is very different from the additional TKE in the two previous wind farm models implemented in WRF. In both these models, the viscous dissipation of TKE is ignored, and the TKE is calculated as the shear production rate multiplied by the time step of the simulation. Both steps lack physical justification.

f. Accounting for missing Reynolds stress

The PBL schemes applied in WRF ignores Reynolds stress $\rho\overline{u_i u_j}$ with only horizontal components ($i, j \neq 3$). This is not justified for cells inside the range of the turbine rotors, where the gradients of the horizontal components must be added to the velocity tendencies in order to be consistent with (1). We lack the means to calculate the non-diagonal horizontal term $\rho\overline{u_1 u_2}$ from the other variables without mixing the turbulence length scale with additional parameters. However, the isotropic turbulence approximation is found to improve in the vicinity of turbines (Gómez-Elvira et al. 2005), which is intuitive. In the isotropic approximation the non-diagonal terms are of course zero and the three diagonal terms are all equal to $q/3$. The final form of the update of the velocity tendency terms is then

$$\frac{\partial U_{k,i}^c}{\partial t} \longrightarrow \frac{\partial U_{k,i}^c}{\partial t} - \frac{T_{k,i}}{\rho\Omega_k} - \frac{1}{3}\frac{\partial q_k^c}{\partial x_i} \tag{52}$$

in the horizontal plane. The numerical absolute value of the last term is bound to be underestimated since the derivative is calculated on the mesoscale. The velocity tendency terms of the two previous wind farm models implemented in WRF, on the other hand, are of the same form as (36).

3. Test case simulations

To illustrate the differences in output from the wind farm model currently implemented in WRF (Jiménez et al. 2015) and the revised model developed in this work, we have conducted ideal simulations of the Horns Rev 1 wind farm with the WRF-system (Skamarock and Coauthors 2008). Observational data are red off figures in the works of Jiménez et al. (2015) and Volker (2014).

We let a hydrostatically balanced flow pass over a flat terrain with water landuse properties. The WRF model has a horizontal resolution of dx=560 m and 41 levels in the vertical, ceiling at 10 km with a 5 km damping zone. The upstream air flow properties is set so that the wind is westerly and the speed is about 8 m/s upwind of the park, the Brunt-Vaisala frequency 0.006 Hz and the moisture content is low so that we avoid saturation. In Figure 1, we present an along-flow cross section at the centre of the park. The fraction of U-momentum and P (power) to the respective value at the first (western most) turbine is presented along with the qke-parameter.

The comparison between our ideal simulations and observations are very sensitive to how the data are processed (e.g. how wide a wind sector we consider, static stability etc.) and how our ideal model setup is done. Even with a careful selection, the data will still show spread (see the Volker-data in Figure 1). This comes from factors we have no control over such as vertical wind shear and transient behaviours. Thus, we do not expect the model to accurately reproduce the power or the momentum curves, but we focus on similarities between model and data development downwind from the first encountered turbine.

In the momentum panel, we see that the new algorithm show a steep drop after the first turbine and some flatter development towards the minimum followed by a quick recovery. The old algorithm gives more of a linear drop from the first turbine towards the minimum. The recovery seems to be slightly slower and weaker. The observations imposed on the plots indicate a clearer "kink" in the curve behind the first turbine. In the power display, we see that the new algorithm clearly flattens out at the minimum whereas the old algorithm show a more linear drop throughout. The old algorithm also goes deeper (beyond 0.5), and this behavior is not supported by the observational data taken from Fig.2d in Jimenez et al. (2015).

4. Conclusion

Physical inconsistencies in the two previous wind farm models implemented in WRF have been addressed, and a revised model has been developed and tested. According to data from the Horn's Rev wind farm, the new model gives a more realistic power development through the wind farm. The steep drop in power or momentum behind the first turbine is still lacking, but this feature is

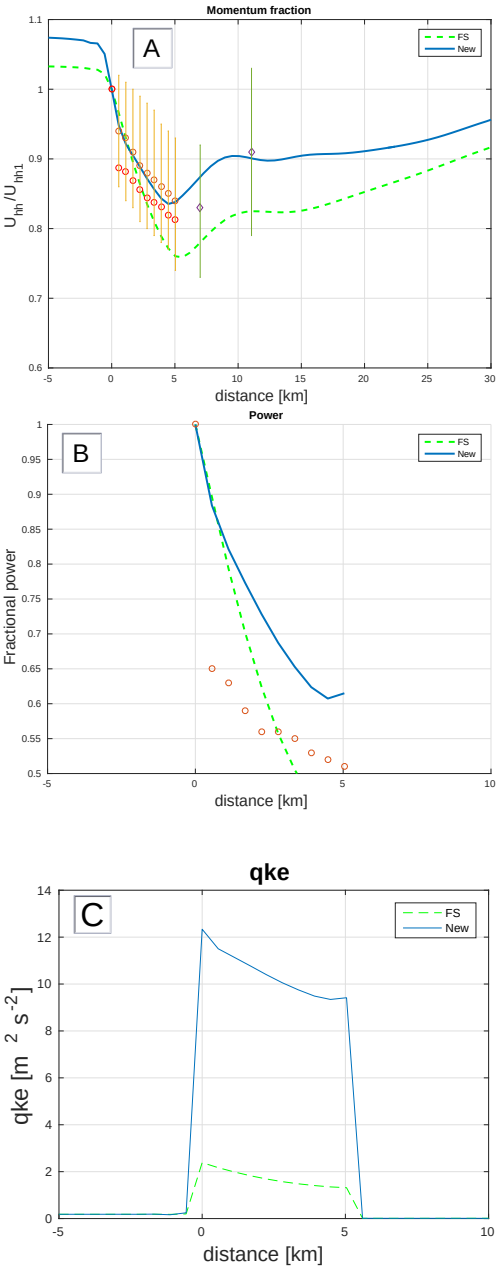

FIG. 1: Comparative plots of relevant variables in an along-flow cross section at the center of the park. Output obtained with the old wind farm algorithm is denoted "FS" and shown as dashed green lines, while "New" refers to output from the algorithm developed in this work shown as solid blue lines.
A) U-momentum as fractions of the value at the most upstream turbine. The Volker-data are the upper circles with bars indicating one standard deviation and diamonds showing mast observations downstream of the park. The Jiménez-data are the lower circles without bars.
B) Power as fractions of the value at the most upstream turbine. Observations shown as circles. Only Jiménez-data exists for this variable.
C) Turbulent kinetic energy represented by the absolute value of $q = qke$. No observations available.

probably not achievable on the mesoscale. A major difference between the new and the previous models is in the calculation of TKE produced by the turbine, which introduces the turbulence length scale as an adjustable parameter in the new model. The TKE is derived from steady state equations, and the velocity tendency terms ignore a non-linearity effect which importance depends on the rate of change in hydrostatic pressure. The revised model may thus be vulnerable to rapid changes in the mean flow, although we expect highly non-adiabatic behaviour to be exceptional on the mesoscale due to the large air masses involved.

Acknowledgments. This work is funded by the NORCOWE consortium (`http://www.norcowe.no/`).

References

Blahak, U., B. Goretzki, and J. Meis, 2010: A simple parameterization of drag forces induced by large wind farms for numerical weather prediction models. *Proc. European Wind Energy Conf. and Exhibition 2010*, PO ID 445, Warsaw, Poland.

Buhl, M. L., 2005: A New Empirical Relationship between Thrust Coefficient and Induction Factor for the Turbulent Windmill State. NREL Technical Report NREL/TP-500-36834.

Burton, T., N. Jenkins, D. Sharpe, and E. Bossanyi, 2011: *Wind Energy Handbook*. 2nd ed., J. Wiley & Sons Ltd, West Sussex, United Kingdom.

Fitch, A. C., J. B. Olson, J. K. Lundquist, J. Dudhia, A. K. Gupta, J. Michalakes, and I. Barstad, 2012: Local and Mesoscale Impacts of Wind Farms as Parameterized in a Mesoscale NWP Model. *Mon. Wea. Rev.*, **140**, 3017–3038, doi:10.1175/MWR-D-11-00352.1.

Frandsen, S., R. Barthelmie, S. Pryor, O. Rathmann, S. Larsen, J. Højstrup, and M. Thøgersen, 2006: Analytical Modelling of Wind Speed Deficit in Large Offshore Wind Farms. *Wind Energy*, **9**, 39–53, doi:10.1002/we.189.

Glauert, H., 1926: The Analysis of Experimental Results in the Windmill Brake and Vortex Ring States of an Airscrew. Aeronautical Research Committee Reports and Memoranda Rept. 1026.

Gómez-Elvira, R., A. Crespo, E. Migoya, F. Manuel, and J. Hernández, 2005: Anisotropy of turbulence in wind turbine wakes. *J. Wind Eng. Ind. Aerodyn.*, **93**, 797–814, doi:10.1016/j.jweia.2005.08.001.

Jiménez, P. A., J. Navarro, and J. Dudhia, 2015: Mesoscale modeling of offshore wind turbine wakes at the wind farm resolving scale: A composite-based analysis with the Weather Research and Forecasting model over Horns Rev. *Wind Energy*, **18**, 559–556, doi: 10.1002/we.1708.

Kundu, P. K., and I. M. Cohen, 2008: *Fluid Mechanics*, chap. 13, 556–559. 4th ed., Academic Press, London, United Kingdom.

Laprise, R., 1992: The Euler equations of motion with hydrostatic pressure as an independent variable. *Mon. Wea. Rev.*, **120**, 197–207.

Lock, C. N. H., H. Batesman, and H. C. H. Townsend, 1926: An Extension of the Vortex Theory of Airscrews with Applications to Airscrews of Small Pitch, Including Experimental Results. Aeronautical Research Committee Reports and Memoranda Rept. 1014.

Nakanishi, M., and H. Niino, 2004: An Improved MellorYamada Level-3 Model with Condensation Physics: Its Design and Verification. *Bound.-Layer Meteor.*, **112**, 1–31.

Schlichting, H., and K. Gersten, 2000: *Boundary Layer Theory*, chap. 18, 558–560. 8th ed., Springer-Verlag, Berlin Heidelberg.

Skamarock, W. C., and Coauthors, 2008: A description of the Advanced Research WRF version 3. NCAR Tech. Note NCAR/TN-475+STR, 133 pp. doi:10.5065/D68S4MVH.

Smith, R. B., 2009: Gravity wave effects on wind farm efficiency. *Wind Energy*, **13**, 449–458, doi:10.1002/we.366.

Volker, P. J. H., 2014: Wake Effects of Large Offshore Wind Farms - a Study of the Mesoscale Atmosphere. Ph.D. thesis, Technical Uiversity of Denmark.

Wilson, R. E., 1994: Aerodynamics of Wind Turbines. *Wind Turbine Technology*, D. A. Spera, Ed., The American Society of Mechanical Engineers, New York, NY, chap. 5, 231–232.